RSC Advances

Accepted Manuscript

ROYAL SOCIETY OF CHEMISTRY

rsc.li/rsc-advances

Journal Name

ARTICLE

The binder-free $Ca_2Ge_7O_{16}$ nanosheet/carbon nanotube composite as a high-capacity anode for li-ion batteries with long cycling life

aaaaReceived 00th January 20xx,
Accepted 00th January 20xx

DOI: 10.1039/x0xx00000x

www.rsc.org/

Xusong Liu,[a] Xiaoxuan Ma,[a] Jing Wang,[a] Xiaoxu Liu,[a,b] Caixia Chi,[a] Shikun Liu,[a] Jiupeng Zhao[a,*] and Yao Li[c,*]

We report a facile one-step route to synthesize a $Ca_2Ge_7O_{16}$ nanosheet(NS)/carbon nanotube(CNT) anode for the first time. The $Ca_2Ge_7O_{16}$ NS/CNT composites are uniformly grown on the surface of three-dimensional Ni foam used as the conductive current collector. The $Ca_2Ge_7O_{16}$ NS/CNT composite is used as a binder-free anode for lithium-ion batteries, which delivers a reversible capacity of 998.5 mA h g^{-1} at a current rate of 0.5 A g^{-1} and exhibits excellent cycle performance (87% retention of its 2nd cycle reversible capacity after 1000 cycles). Furthermore, a binder free full cell is fabricated, which shows excellent cycle performance with 96% retention of its 10th cycle capacity after 100 cycles. The superior cycling performance is attributed to the synergetic effect of small diffusion lengths in NS, sufficient void space to buffer the volume expansion, the CNT for charge transport and a continuous 3D electronic path of the Ni foam.

Introduction

Lithium-ion batteries (LIBs) have been widely utilized in portable electronic devices, electric vehicles and power tools, because of their high energy density, high rate capability, high safety and low cost.[1,2] However, the commercial graphite materials used as the anode materials of lithium-ion batteries have a low theoretical capacity (372 mA h g^{-1}), which limits the application of LIBs.[3,4,5] From the viewpoint of energy density, group IVA elements are the most promising materials, especially Si and Ge, which can deliver theoretical capacities of 4200 mA h g^{-1} (volumetric capacity of 8344 A h L^{-1}) and 1600 mA h g^{-1} (volumetric capacity of 7366 A h L^{-1}), respectively.[6] Compared with Si-based materials, Ge exhibits a higher diffusivity of lithium (400 times faster than Si), a lower specific volume change and high intrinsic electrical conductivity (100 times higher than Si) during the Li insertion/extraction process, which can be expected to lead to a better cycling performance at comparable capacity.[7,8] However, Ge still undergoes a volume change of 370%.[9] To minimize such volume strain during the charge and discharge processes, we have devoted to creating germanium nanostructures that can accommodate the lithiation induced strain and thus exhibit high coulombic efficiency and long cycle life.[10,11,12]

Another issue that must be addressed here is the problem of feasibility as Ge is not an abundant or inexpensive material.[13] Despite its advantages, Ge has received less attention than the more widely investigated Si, mainly because of its high cost.[14] Therefore, to discover a stable and high capacity Ge-based compound, earth-abundant elements would be the best solution to cover all problems mentioned above. In recent years, the ternary Ge compounds ($MGeO_3$, where M= Cu, Fe and Co) electrodes are regarded as promising anodes for LIBs, which generate nanosized metallic M particles that make an intimate contact with the nano-sized Ge ($CuGeO_3 + 2Li^+ + 2e^- \rightarrow Cu + Li_2O + GeO_2$, $GeO_2 + 4Li^+ + 4e^- \rightarrow Ge + 2Li_2O$) and Li_2O, that they can catalyze Li_2O decomposition ($Ge + 2Li_2O \rightarrow GeO_2 + 4Li^+ + 4e^-$) and provide an electronic conductive network for Ge oxidation.[15] From then on, germanate containing metal elements (Zn[13,16], Cu[17], Ba[18], Sr[18], Cd[19], Fe[20]) have been reported for lithium storage. $Ca_2Ge_7O_{16}$ has demonstrated its promising potential for applications in high performance LIBs for low-cost, environmentally benign, and good stabilized matrix.[14,18,21,22] The CaO formed in situ (CaO for $Ca_2Ge_7O_{16}$) after the initial delithation process, accompanied by the formation of Li_2O, can not only serve as a buffer matrix to accommodate the volume changes in the germanium nanoparticles, but also effectively prevent the agglomeration of the nanosized germanium particles that are formed during the process. For example, Guo et al.[18] showed the better cycling performance of $Ca_2Ge_7O_{16}$ nanowires with a specific capacity of 601 mA h g^{-1} after 100 cycles under a current density of 100 mA g^{-1} than $BaGe_4O_9$ nanowires and GeO_2. However, the coulombic efficiency (CE) in the first cycle of $Ca_2Ge_7O_{16}$ nanowires is 18.1%, which is lower than $BaGe_4O_9$ nanowires (25.6%) and GeO_2 (33%). Shen et al.[21] showed improved cycling performance of the $Ca_2Ge_7O_{16}$ nanowires/graphene anodes with a specific capacity of 950 mA h g^{-1} at a current density of 100

[a] MIIT Key Laboratory of Critical Materials Technology for New Energy Conversion and Storage, School of Chemistry and Chemical Engineering, Harbin Institute of Technology, 150001, Harbin, China. E-mail: jpzhao@hit.edu.cn
[b] Heilongjiang university of Science and Technology, Harbin 150027, China.
[c] Center for Composite Material, Harbin Institute of Technology, 150001, Harbin, China. E-mail: yaoli@hit.edu.cn

† Electronic Supplementary Information (ESI) available: Crystal structure of the $Ca_2Ge_7O_{16}$, TG results, N_2 adsorption-desorption, Discharge-charge profiles, SEM and a simple application of a $Ca_2Ge_7O_{16}$ NS/CNT composite. See DOI: 10.1039/x0xx00000x

mA g^{-1} after 100 cycles and a higher CE (45%). The $Ca_2Ge_7O_{16}$ hollow microspheres which were prepared by Guo et al. exhibited the superior electrochemical properties with a specific capacity of 804.6 mA h g^{-1} at a current density of 100 mA g^{-1} after 100 cycles and the CE was less than 50%.[22] However, these $Ca_2Ge_7O_{16}$ electrodes had relatively low CE and short cycling life under a lower current density (100 mA g^{-1}) due to the pulverization caused by the volume expansion and poor electronic conductivity. Therefore, the synthesis of $Ca_2Ge_7O_{16}$ with well-defined nanostructures and excellent lithium storage capacity remains a great challenge owing to the volume expansion of $Ca_2Ge_7O_{16}$.

The NS electrodes have showed many advantages, such as good electrical conductivity, low diffusion resistance to ionic species, easy electrolyte penetration, and large electroactive area.[23,24] At the same time, the presence of the voids between the NS structures will not only relieve the structural alterations caused by the charge-discharge process, thus improving the cycling performance, but also help to store more lithium. CNT with high conductivity, large specific surface area and superior mechanical properties, can provide a support for anchoring nanocrystals and work as a highly conductive matrix.[25,26]

Here, we present a unique nanostructure composed of $Ca_2Ge_7O_{16}$ NS/CNT composite, which was synthesized by a simple, fast and high yield hydrothermal method for the first time. The as-prepared nanostructure electrode can not only shorten the ion-diffusion length and support fast electron transport, but also is favorable for alleviating mechanical stress and maintaining the structural integrity of the electrode. This $Ca_2Ge_7O_{16}$ NS/CNT electrode exhibits excellent cycle performance (87% retention of its 2nd cycle capacity after 1000 cycles at 0.5 A g^{-1}), an outstanding initial discharge capacity of 1855 mA h g^{-1} at current density of 200 mA g^{-1}. To our knowledge, there are no reports on $Ca_2Ge_7O_{16}$-based anodes capable of cycling up to 1000 cycles until now. After the rate performance test, the coin cell is cycled for additional 100 cycles at 0.1 A g^{-1}, maintaining a capacity of 1001.6 mA h g^{-1} (99.44% of the sixth cycle reversible capacity), which further confirms the excellent cyclic performance of this $Ca_2Ge_7O_{16}$ NS/CNT composite anode. We use the $Ca_2Ge_7O_{16}$ NS/CNT as the anode and the commercial $LiCoO_2$ (LCO) material as the cathode to assemble a $Ca_2Ge_7O_{16}$ NS/CNT/LCO full cell. The binder free full cell exhibits excellent cycle performance with 96% retention of its 10th cycle capacity after 100 cycles.

Experimental

Chemicals

High purity reagent GeO_2 powders (purity ≥ 99.99%) and $Ca(CH_3COO)_2{\cdot}H_2O$ (AR grade, purity ≥ 98.0%) were purchased From Shanghai Longjin Metallic Material Co., Ltd. and Sinopharm Chemical Reagent Co., Ltd. of China, respectively. High purity CNTs (20-30 nm) were purchased From Beijing Boyu New Material Co., Ltd. Ni foam and commercial $LiCoO_2$ were purchased From Shenzhen Biyuan Electronic Co., Ltd.

Synthesis of the $Ca_2Ge_7O_{16}$ NS

In a typical procedure, 176 mg GeO_2 and 366.1 mg $Ca(CH_3COO)_2{\cdot}H_2O$ were dissolved in 30 mL deionized water, respectively. The mole ratio of Ca:Ge is 2. The $Ca(CH_3COO)_2{\cdot}H_2O$ solution was added dropwise to GeO_2 solution under vigorous stirring. The mixture was stirred for 60 min and then transferred to a Teflon-lined auto-clave with a 100 mL inner volume. Then a piece of cleaned Ni foam was placed into the solution. The hydrothermal synthesis was performed at 180℃ for 20 h, followed by natural cooling to room temperature. The white product was collected by centrifugation, washed thoroughly with water and alcohol several times and then dried at 60℃ in air for 12 h. Finally, the $Ca_2Ge_7O_{16}$ NS Ni foam was obtained.

Synthesis of the $Ca_2Ge_7O_{16}$ NS/CNT

CNTs were refluxed in a mixed solution of concentrated HNO_3 and H_2SO_4 overnight to open the CNTs tips. After filtering, washing with pure water and drying, the open CNTs were obtained. In a typical procedure, 30 mg acid-treated CNTs were dissolved in 30 mL deionized water by mild ultra-sonication for 1 h. Then 176 mg GeO_2 and 366.1 mg $Ca(CH_3COO)_2{\cdot}H_2O$ were added into resultant solution, respectively. The mole ratio of Ca:Ge is 2:1. The $Ca(CH_3COO)_2{\cdot}H_2O$ solution was added dropwise to resultant solution under vigorous stirring. The mixture was stirred for 60 min and then transferred to a Teflon-lined auto-clave with a 100 mL inner volume. Then a piece of cleaned Ni foam was placed into the solution. The hydrothermal synthesis was performed at 180℃for 20 h, followed by natural cooling to room temperature. The product was collected by centrifugation, washed thoroughly with water and alcohol for several times and then dried at 60℃in air for 12 h. Finally, the $Ca_2Ge_7O_{16}$ NS/CNT Ni foam nanocomposite was obtained.

Characterization

The morphology and element distribution of the electrodes were investigated by field emission-scanning electron microscopy (FE-SEM; Hitachi S-4800) operating at 20 kV. Transmission electron microscopy (TEM) was performed using an FEI Tecnai G2F30 operated at 300 kV. X-Ray diffraction (XRD) measurements were performed at a Rigaku D/max-rB X-ray diffractometer with Cu Kα (λ=0.1548 nm) incident radiation. The diffraction patterns were collected at room temperature in the 2ɵ ranges of 10 to 90°. Raman spectroscopy was performed with a laser micro Raman spectrometer (RenishawinVia, Renishaw, 532 nm excitation wavelength). An X-ray photoelec-tron spectroscopy (XPS) study was conducted with a PHI 5700 ESCA System using Al Kα radiation (1486.6 eV). Thermogravimetric (TG) analysis was performed on a SDT Q 600 V 20.9 Build 20 TG/DTA apparatus at a heating rate of 10℃ min^{-1} in flowing air. Brunauer-Emmett Teller (BET) analysis was carried out using a N_2 adsorption-desorption apparatus (3H-2000PS1, Bass).

Electrochemical charge-discharge behaviors were investigated in stimulant cells (2032 coin-type half-cells) assembled with $Ca_2Ge_7O_{16}$ NSs/CNTs composite as the positive electrode (cathode), a Li metal foil as the negative electrode (anode), a separator film (Celgard 2400), and a liquid electrolyte (ethylene carbonate and dimethyl

carbonate (1:1 by volume)) with 1.0-M $LiPF_6$ in an Ar filled glove box. The loading density of the $Ca_2Ge_7O_{16}$ NS/CNT active materials was calculated to be 1.0-2.0 mg cm^{-2}. Each cell was aged for 24 h at room temperature before commencing the electrochemical tests. The galvanostatic charge-discharge measurements were conducted in a battery test system (NEWARE BTS-610, Newware Technology Co., Ltd., China) at room temperature. The cut-off voltage for all tests was 0.01-3.0 V. A full cell was assembled by using the as-fabricated $Ca_2Ge_7O_{16}$ NSs/CNTs as the anode, commercial $LiCoO_2$ as the cathode, $LiPF_6$ as the electrolyte, and a polymer separator. The electrochemical tests were cycled between 2.0 and 4.2 V for the complete anode-limited full cells at a constant current density of 200 mA g^{-1} with respect to the mass of the anode. Cyclic voltammograms (CV) were measured at a scan rate of 0.1 mV s^{-1} for 5 cycles on an electrochemical work station (CHI660E). AC impedance of the half-cells was also performed on an electrochemical work station (CHI660E) at a frequency range of 100 mHz-100 kHz. All testing was performed at room temperature.

Results and discussion

The synthetic process of the $Ca_2Ge_7O_{16}$ NSs/CNTs nanocomposite is schematically illustrated in Figure 1. Firstly, $HGeO^{3-}$ was formed from the reaction of GeO_2 and OH^- which came from CH_3COO^-. Then free Ca^{2+} ions which derived from $Ca(CH_3COO)_2{\cdot}H_2O$ reacted with $HGeO^{3-}$, and finally the $Ca_2Ge_7O_{16}$ nucleis generated on Ni foam (Fig.1 a). As the reaction time prolonged, the $Ca_2Ge_7O_{16}$ nucleis started to assemble along the specific orientation preferentially and formed the $Ca_2Ge_7O_{16}$ NS (Fig.1b). The CNTs were adhered on the surface of the $Ca_2Ge_7O_{16}$ NSs through electrostatic interaction to form the $Ca_2Ge_7O_{16}$ NS/CNT nanocomposites.

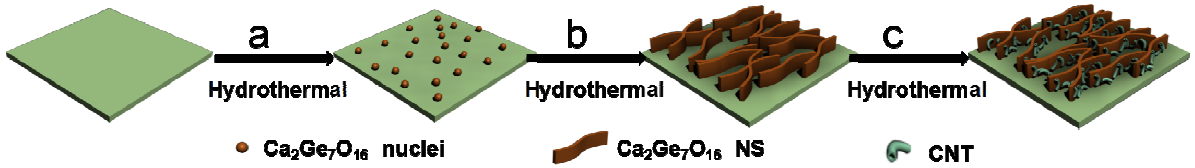

Figure 1. Schematic diagram for the preparation of the $Ca_2Ge_7O_{16}$ NS/CNT nanocomposite. (a). GeO_2 reacted with $Ca(CH_3COO)_2{\cdot}H_2O$ to form the $Ca_2Ge_7O_{16}$ nucleis on Ni foam by hydrothermal method at 180□. (b). The $Ca_2Ge_7O_{16}$ nucleis started to assemble and form $Ca_2Ge_7O_{16}$ NSs. (c). The CNTs were adhered on the surface of the $Ca_2Ge_7O_{16}$ NSs.

The crystalline structure of the $Ca_2Ge_7O_{16}$ NS/CNT nanocomposite was characterized by XRD and the results are shown in Fig. 2 a. All of the diffraction peaks can be well indexed to the orthorhombic phase of $Ca_2Ge_7O_{16}$ (JCPDS Card No. 34-0286). Diffraction peaks which might appear for the CNTs are absent; most likely the CNT peaks are eclipsed by those for $Ca_2Ge_7O_{16}$. The crystallographic structure of the orthorhombic $Ca_2Ge_7O_{16}$ is shown in Fig. S1 † Fig. 2 b shows Raman spectrum of the $Ca_2Ge_7O_{16}$ NS/CNT nanocomposite. The characteristic D band and G band of the $Ca_2Ge_7O_{16}$ NS/CNT are observed at 1349.4 cm^{-1} and 1583.1 cm^{-1}, respectively. The D-band is commonly assigned to a breathing mode of A1g symmetry that involves phonons near the K-zone boundary, and the G-band corresponds to the zone center E2 mode which is related to phonon vibrations in sp^2 carbon materials.[27] Fig. S2 † shows the carbon content in the $Ca_2Ge_7O_{16}$ NS/CNT nanocomposite is evaluated to be ca. 19.5% by TG analysis. Fig. 2 c shows the general XPS spectrum of the $Ca_2Ge_7O_{16}$ NS/CNT nanocomposite, which includes the elements C, Ge, Ca and O. The C 1s spectrum (Fig. 2 d) could be divided into four peaks corresponding to the C-C (sp^2 C), C-O, C=O, and O-C=O groups at 284.5, 285.3, 286.4 and 290.7 eV, respectively. As shown in Fig. S3 †, the peak at 32.1 eV is assigned to Ge 3 d, indicating that Ge in the sample exists in the form of Ge^{4+} before the cycle.[28]

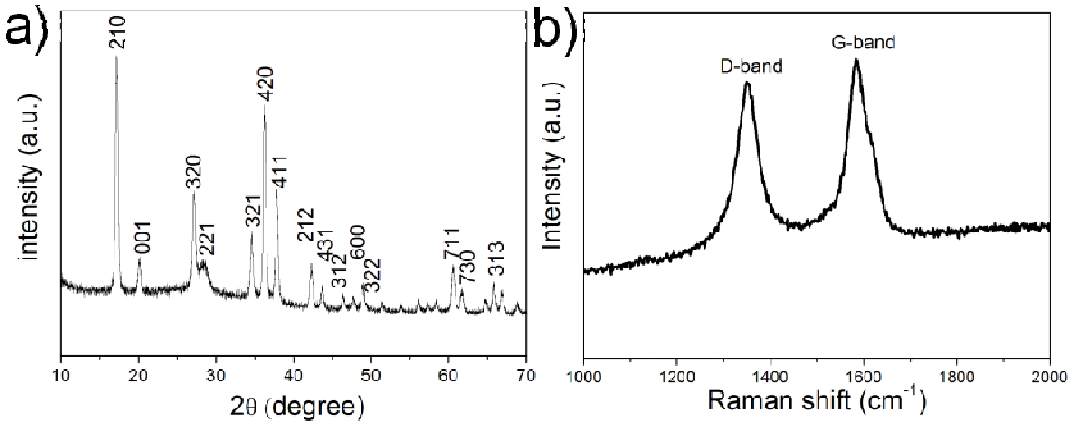

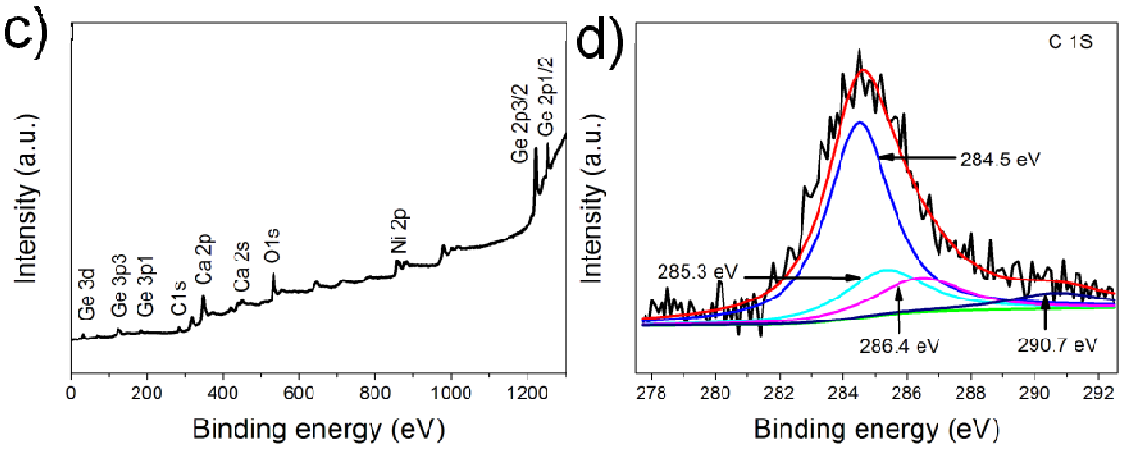

Figure 2. (a) XRD pattern; (b) Raman spectrum; (c) Survey XPS spectrum; (d) High-resolution XPS spectrum of C 1s of the as-prepared $Ca_2Ge_7O_{16}$ NS/CNT nanocomposite.

Fig. 3 shows the morphology the $Ca_2Ge_7O_{16}$ NS/CNT nanocomposite supported on the Ni foam. It reveals that a large number of $Ca_2Ge_7O_{16}$ NS/CNT nanocomposites with the thickness ranging from 20-40 nm grow vertically and uniformly on the Ni foam, forming an interconnected and highly porous configuration. CNTs with the length of about 50-150 nm are well distributed on the surface of the $Ca_2Ge_7O_{16}$ NSs. The porous structure of the composite was further evaluated by BET N_2-adsorption-desorption analysis (Fig. S4 †). Such NS structure gives rise to a relatively high BET specific surface area of 39.22 m^2g^{-1}. With the benefits of the porous structure and the introduction of conductive CNTs, the composite is believed to be advantageous to high ion accessibility, fast ion and electron transport.

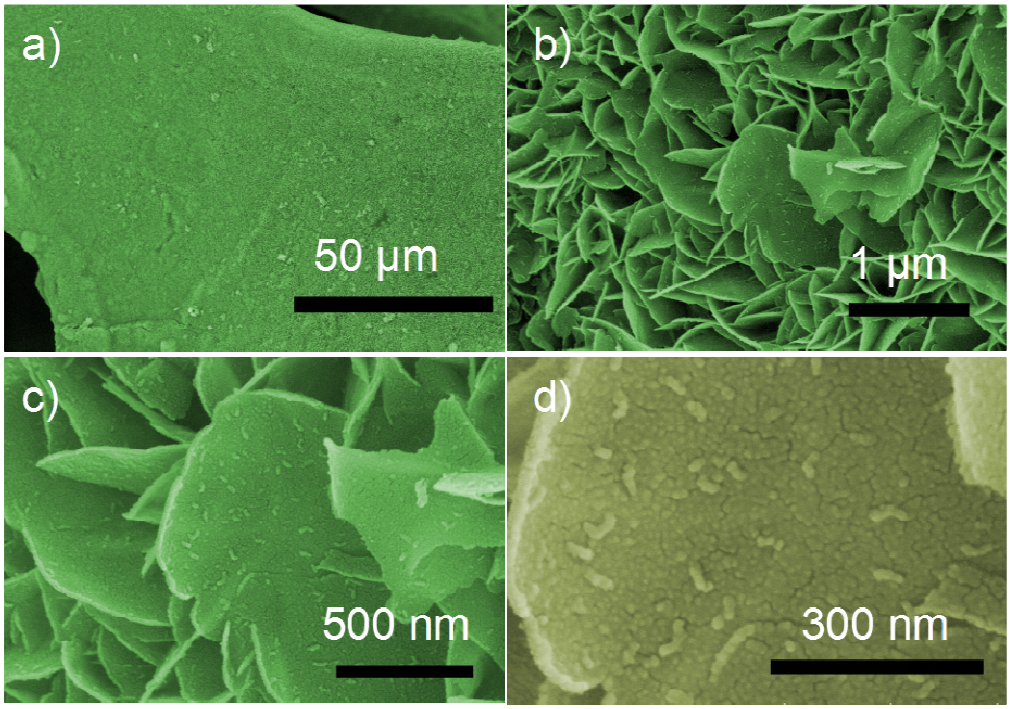

Figure 3. (a-d) SEM images of the $Ca_2Ge_7O_{16}$ NS/CNT nanocomposite at various magnifications.

More detailed structural information and morphology of $Ca_2Ge_7O_{16}$ NS/CNT were investigated by TEM. The TEM images of $Ca_2Ge_7O_{16}$ NS/CNT in Fig. 4a,b confirm that the average thickness of the NS is about 20-40 nm which is consistent with the result of SEM. CNTs with the diameter of about 20-30 nm are distributed on the surface of the $Ca_2Ge_7O_{16}$ NSs. Fig. 4 c shows High-resolution TEM (HRTEM) image of the vertical edge of a $Ca_2Ge_7O_{16}$ NS perpendicular to basal surface of NSs, which is attributed to folding and curving of NSs (highlighted by the white square line in Fig. 4 a). It shows lattice fringes with spacing of 8.01 Å corresponding to the

(110) lattice of a $Ca_2Ge_7O_{16}$ NS. Figure 4 d shows lattice fringes with spacing of 4.02 Å and 3.59 Å, corresponding to the (111) and (021) lattice planes of a $Ca_2Ge_7O_{16}$ NS (the area highlighted by the black square line in Fig. 4 a), respectively. The SAED pattern (the inset of Figure 4 a) shows the as-prepared $Ca_2Ge_7O_{16}$ NS is polycrystalline in nature.

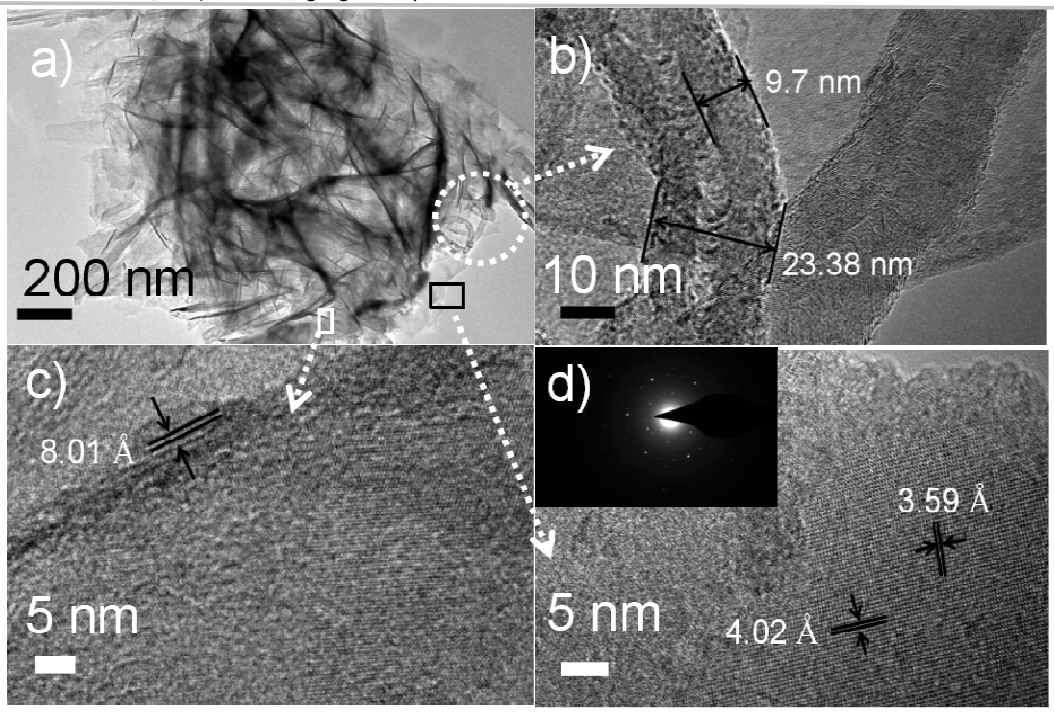

Figure 4 (a) Low-resolution TEM image of the $Ca_2Ge_7O_{16}$ NS/CNT nanocomposite. (b) High-resolution TEM image of the area highlighted by the white circle of (a). (c) and (d) HRTEM images of the $Ca_2Ge_7O_{16}$ NS. The inset shows the SAED image of (d).

Figure 5a shows the CV curves of $Ca_2Ge_7O_{16}$ NS/CNT anode, which is used to investigate the lithium insertion-desertion mechanism in the electrode. In the initial sweep, there is a remarkable cathodic peak located around 0.97 V which is ascribed to the decomposition of $Ca_2Ge_7O_{16}$ into Ca, Ge, Li_2O and the formation of the SEI film. Other peaks at 0.69 V and 0.2 V indicate the Li-Ge alloying reactions (Figure 5a). In the anodic-scan process, a broad peak centered at 0.52 V can be assigned to the delithation of the Li-metal alloys. Of particular note, three peaks located at 1.05 V, 1.3 V and 2.2 V represent the reoxidation of Ge, corresponding to the conversion reaction.[29, 30] For the subsequent cycles, two main reduction peaks in the range of 0.5 V to 1.0 V and 0 to 0.5 V are observed which correspond to Li-Ge alloying reactions. The reduction peaks in the range of 1.5 V to 1.75 V is corresponding to the reduction of GeO_2 to Ge. During the anodic potential sweeps, broad oxidation peaks around 0.5 V are observed, which are associated with the delithation. The oxidation peaks at 1 V to 2.5 V are associated with the reoxidation of Ge to GeO_2. The overall electrochemical reaction process during Li insertion/extraction can be described as follows:

$$Li^+ + e^- + \text{electrolyte} \rightarrow \text{SEI (Li)}$$

$$Ca_2Ge_7O_{16} + 28e^- + 28Li^+ \rightarrow 2CaO + 7Ge + 14Li_2O \text{ (0.97 V)}$$

$$Ge + xe^- + xLi^+ \leftrightarrow Li_xGe \ (0 \le x \le 4.4, \text{ 0 V - 0.7 V})$$

$$Ge + Li_2O \leftrightarrow GeO_2 + 4Li^+ + 4e^- \text{ (1 V - 3 V)}$$

Fig. 5 b shows the representative galvanostatic charge/discharge profiles of the electrode at a current density of 500 mA g^{-1} after 5 cycles activation at 200 mA h g^{-1} within a cut-off voltage window between 0.01 and 3 V. All the galvanostatic discharge-charge voltage profiles with the consistent voltage platform indicate the stable electrochemical processes as those in the CV measurements (Fig. 5 a). The discharge and charge capacities at the 1st, 2nd, 100th, 300th, 500th, 800th, 1000th cycles are 1002.2 and 998.5, 815.4 and 749.7, 626.7 and 612.7, 508.6 and 500, 717.8 and 711.8, 725.5 and 720.8, 652.6 and 652.1 mA h g^{-1} at a current density of 500 mA g^{-1}, respectively, as shown in Fig. 5 b. The first discharge and charge capacity is 1855.7 and 1263.4 mA h g^{-1}, respectively. Fig. 5 c gives the long-term cycling performance of the $Ca_2Ge_7O_{16}$ NS/CNT at a current rate of 500 mA g^{-1} after 5 cycles activation at a current rate of 200 mA g^{-1}. Our $Ca_2Ge_7O_{16}$ NS/CNT anode exhibits a superior cycling performance, delivering a high reversible capacity of 724.2 mA h g^{-1} even after 800 cycles, which is much higher than the previous report.[22] After 1000 cycles, the capacity retention is 87% of its 2nd cycle reversible capacity (dropping by only 0.01% per cycle) at 500 mA g^{-1}. The capacity gradually decreases first and then increases (after about 300 cycles), which can be attributed to the reversible formation of a polymeric gel-like layer via electrolyte decomposition, further activation of active materials and the electrocatalytic reversible conversion of some components of SEI films. The phenomenon is usually observed in transition metal oxides anode materials.[31,32] Even cycled at a high current density of 1 A g^{-1} after 500 cycles, the reversible specific capacity of the electrode is still as high as 600.3 mA h g^{-1}, indicating the excellent cycling performance (Fig. S5 a and b †). The first CE of the $Ca_2Ge_7O_{16}$ NS/CNT anodes is 68.1%, which is

much higher than the previous reports,[18, 21] as shown in Fig. 5 d. Then, it increases to 98% in the next cycle and reaches a stable value of almost 100% after 10 cycles, indicating a very high reversibility of the $Ca_2Ge_7O_{16}$ NS/CNT anode. The initial capacity loss is caused by incomplete conversion and the formation of a solid electrolyte interphase (SEI) layer ascribed to the electrolyte decomposition (Fig. S6 a †, highlighted by the white line).[33] After lithiation, the electrode can maintain an integrated structure without pulverization and fracture (Fig. S6 b †), resulting in a stable cycle performance. For comparison, the lithium-storage performance of the pristine $Ca_2Ge_7O_{16}$ NS electrode was also studied. The pristine $Ca_2Ge_7O_{16}$ NS electrodes with the thickness about 20-40 nm grow on the Ni foam uniformly (Fig. S7 †). By contrast, the capacity (768.75 mA h g^{-1}) begins to decrease rapidly at 50th cycle, and retains 427.75 mA h g^{-1} after 200th cycles at 500 mA g^{-1}. After cycling, the pristine $Ca_2Ge_7O_{16}$ NS suffers pulverization and fracture caused by volume variation (Fig. S8 †).

To further investigate the electrochemical performance of the $Ca_2Ge_7O_{16}$ NS/CNT composite, the rate performance was examined. The rate capability of $Ca_2Ge_7O_{16}$ NS/CNT composite in the applied current range of 0.1-5 A g^{-1} is shown in Fig 5e. The $Ca_2Ge_7O_{16}$ NS/CNT electrode exhibits charge capacity (reversible capacity) of 1396.3, 919.8, 714.1, 539.1, 342.4, 200 mA h g^{-1} at rates of 0.1, 0.2, 0.5, 1, 2, 5 A g^{-1}, respectively. As expected, the $Ca_2Ge_7O_{16}$ NS/CNT electrode exhibits a better rate performance compared with the NS electrode (Fig. S9 †). When the rate returns back to 100 mA g^{-1} after 100 cycles, the charge capacity can be largely recovered which indicate a good rate performance. A CE is almost 100% for all the cycles except the first cycle due to the formation of a SEI as mentioned previously. After the rate performance test, the coin cell is cycled for additional 100 cycles at 0.1 A g^{-1}, maintaining the capacity of 1001.6 mA h g^{-1} (99.44% of the sixth cycle reversible capacity), which further confirms the excellent cyclic performance of the $Ca_2Ge_7O_{16}$ NS/CNT composite anode. The good capability and excellent cycling stability of the $Ca_2Ge_7O_{16}$ NS/CNT electrode are impressive values when compared to those of many previously reported $Ca_2Ge_7O_{16}$ based electrodes, as shown in Table S1†.

Several contributing factors can be considered for the high specific capacity and excellent cycling stability of the $Ca_2Ge_7O_{16}$ NS/CNT composite anode. First, the NS structures greatly shorten the ionic diffusion length and provide sufficient electrode-electrolyte contact area for lithium-storage reactions. The presence of the voids between the NS structures will not only relieve the structural alterations caused by the charge-discharge process, thus improving the cycling performance, but also help to store more lithium. Second, the incorporation of CNTs can improve the mechanical strength and increase the electronic contact and conductivity of the anode.[34] Last, the nickel foam also plays an important role in enhancing the electrode conductivity by forming a continuous 3D electronic path for fast and stable charge transfer while providing the electrode with a large specific surface area, high porosity, and high mechanical flexibility.

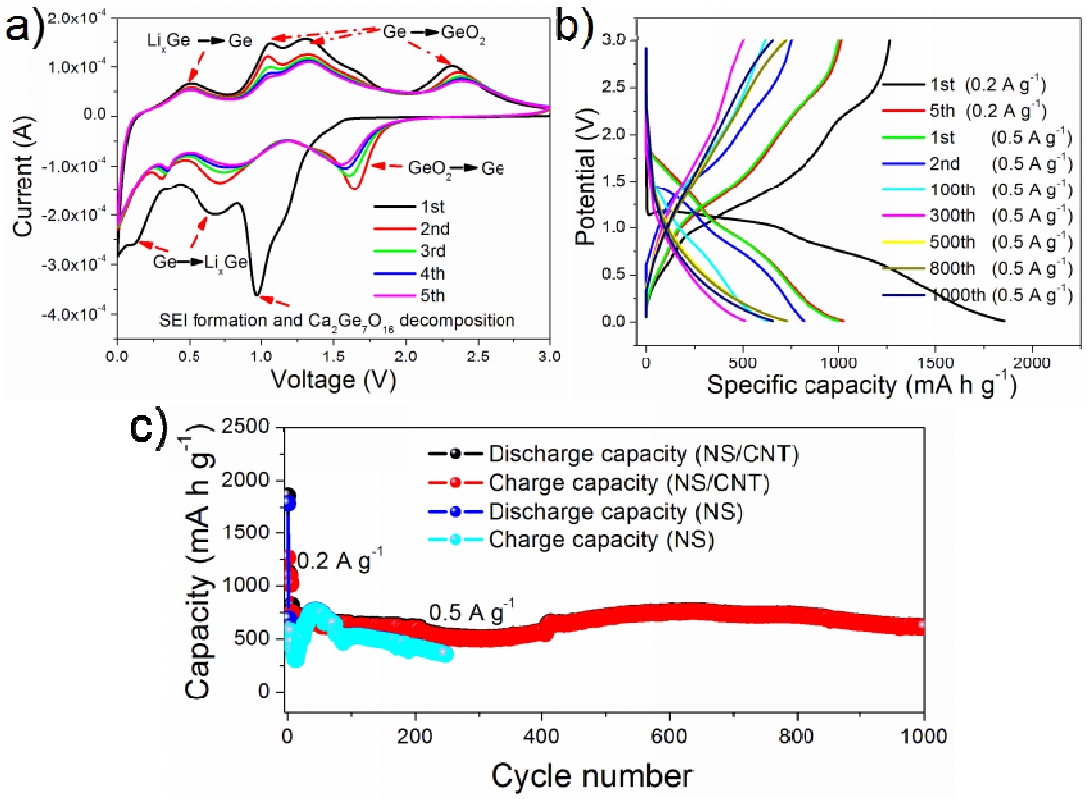

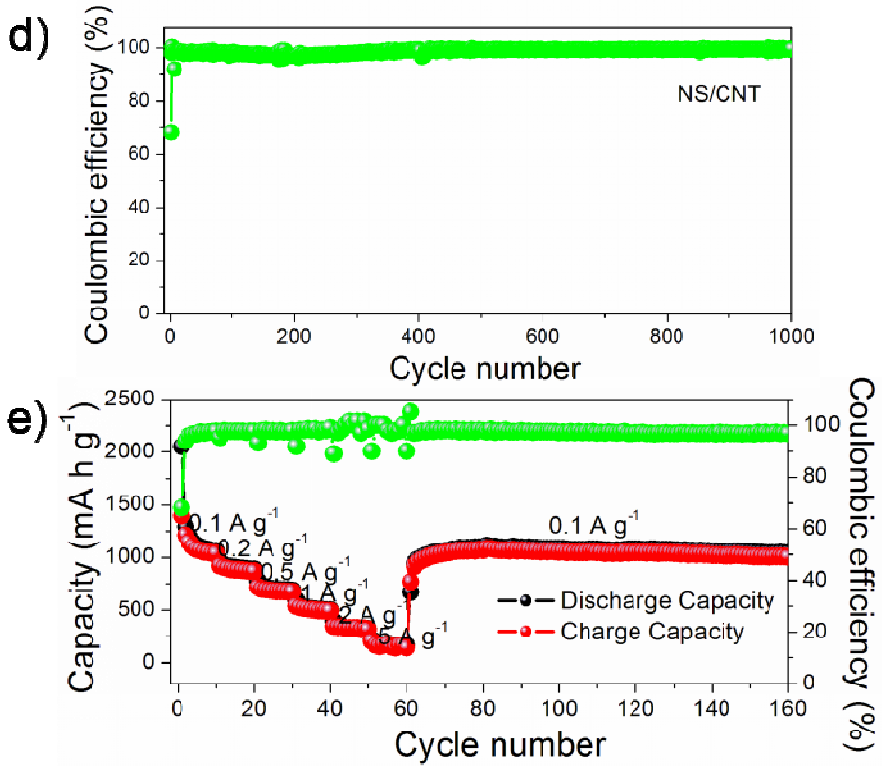

Figure 5 (a) CV curves and (b) discharge/charge profiles of the $Ca_2Ge_7O_{16}$ NS/CNT anode. (c) Cycling performances of different samples at 500 mA g^{-1} after 5 cycles activation at 200 mA g^{-1} between 0.01 and 3 V. (d) CE of the $Ca_2Ge_7O_{16}$ NS /CNT anode. (e) Rate performance of the $Ca_2Ge_7O_{16}$ NS /CNT anode.

The enhanced ion diffusion and effective electron transfer in the composite electrode are further confirmed by the EIS measurements, which were performed in the frequency range between 100 kHz and 10 mHz before the charge and discharge process (Figure 6). The fitting of EIS data was carried out with a Zview software. The experimental result at the fully discharged state was fitted by a one time-constant equivalent circuit. The data of the Nyquist plots were analyzed by fitting to equivalent electric circuit (EEC), as shown in Fig. 6 a. The EIS spectra of the $Ca_2Ge_7O_{16}$ NS/CNT anode show the compressed semicircle from the high to medium frequency range of each spectrum, which describes the resistance of SEI and charge transfer (R2) and constant-phase element (CPE1, representing the double-layer capacitance) for the electrodes. A line inclined at approximately 45° at the low frequency, corresponding to the Warburg impedance (W) that is related to the Li^+ ions diffusion. On the basis of a simplified equivalent circuit the estimated R2 value of the $Ca_2Ge_7O_{16}$ NS/CNT (78.4 Ω) is relatively lower than that of the pristine $Ca_2Ge_7O_{16}$ NSs (118.1 Ω), indicating the improved charge transport properties of the $Ca_2Ge_7O_{16}$ NS/CNT due to the combination of CNT as a conducting medium. The lithium diffusion coeffcient of the $Ca_2Ge_7O_{16}$ NS/CNT electrode is calculated to be 4.98×10^{-13} cm^2 s^{-1}, indicating a fast lithium ion diffusion process (Fig. S10 †).

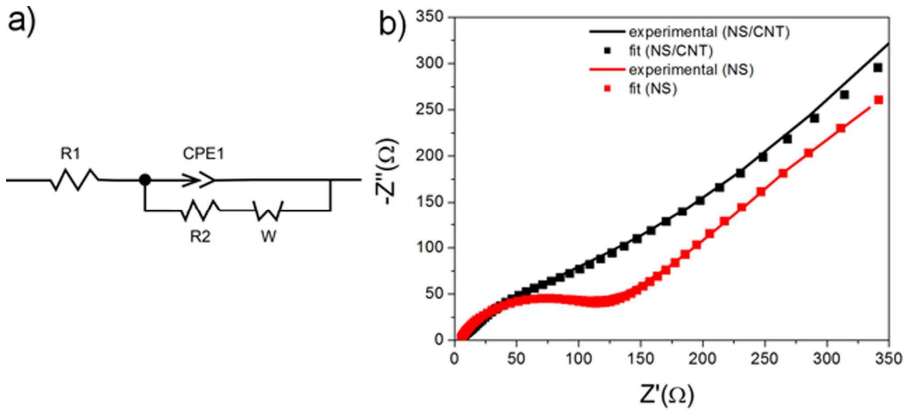

Figure 6 (a) Equivalent circuit model of the $Ca_2Ge_7O_{16}$ NS/CNT anode. (b) Typical Nyquist plots and fitted EIS plot of the pristine $Ca_2Ge_7O_{16}$ NS and the $Ca_2Ge_7O_{16}$ NS/CNT.

By using this $Ca_2Ge_7O_{16}$ NS/CNT as an additive-free anode and commercial $LiCoO_2$/Al foil as a cathode, we fabricated a coin-type full cell. The electrochemical performance of the anode-limited full cell (that is, when considering the matching of the electrodes, the capacity of the anode is appropriately lower than that of the cathode) was investigated by cycling within the voltage range of 2.0-4.2 V at a current density of 0.2 A g^{-1}. After packed, the full cell was subjected to a pre-lithiation cycle by charging and discharging at a low current density. According to a previous report, this procedure should form a solid electrolyte interphase (SEI) layer on the surface of the anode owing to decomposition of the electrolyte.[35] Figure 7 a shows the voltage-capacity profiles of the full cell device for the 1st, 2nd, 10th, 30th, 50th, 80th and 100th charge/discharge cycles with a discharge voltage plateau of about 3.6 V and a charge-voltage plateau of about 3.7 V. The reversible capacities at the 1st, 2nd, 10th, 30th, 50th, 80th and 100th cycles are 1703.7, 1477.1, 1247.8, 1290.7, 1253.6, 1219 and 1197.8 mA h g^{-1}, respectively. The binder free full cell exhibits excellent cycle performance with 96% retention of its 10th cycle capacity after 100 cycles (Figure 7 b). To evaluate the potential application of the $Ca_2Ge_7O_{16}$ NS /CNT electrodes for LIBs, the output voltage of the as-prepared full cell is found to be 4.19 V, which can give a larger current intensity (~120 mA) to light up 6 commercial blue LEDs, Figure S11 †. Thus, it is expected that the $Ca_2Ge_7O_{16}$ NS /CNT can be utilized as a promising alternative anodic material in LIBs.

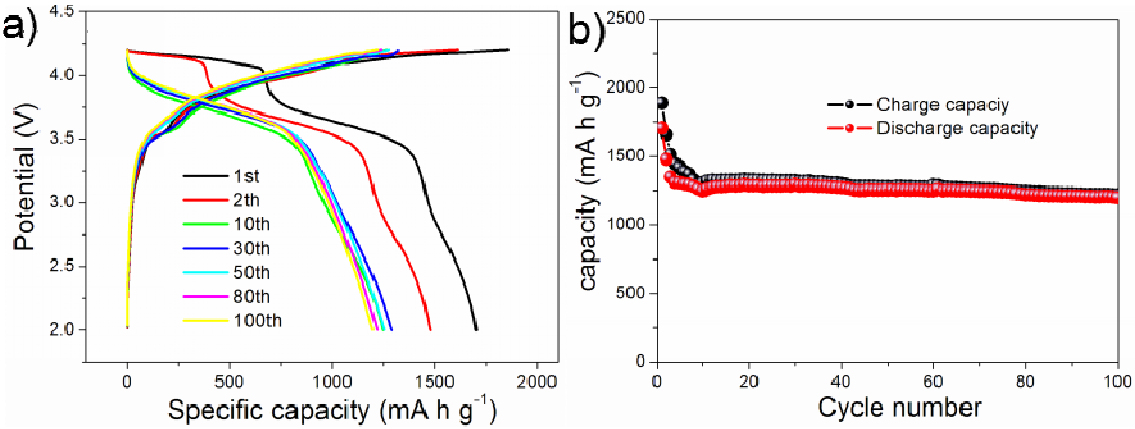

Figure 7 Electrochemical characterization of the $Ca_2Ge_7O_{16}$ NS/CNT/$LiCoO_2$ full-cell. (a) Discharge/charge profiles and (b) Cycling performance measured at a current density of 0.2 A g^{-1} for the $Ca_2Ge_7O_{16}$ Ns/CNT/$LiCoO_2$ full-cell.

Conclusions

In conclusion, a $Ca_2Ge_7O_{16}$ NS/CNT anode has been fabricated via a simple, fast and high yield hydrothermal method for the first time. The $Ca_2Ge_7O_{16}$ NS/CNT composites are uniformly grown on the surface of three-dimensional Ni foam. CNTs with the length of about 50-150 nm are well distributed on the surface of the $Ca_2Ge_7O_{16}$ NSs with the thickness ranging from 20-40 nm. The as-prepared $Ca_2Ge_7O_{16}$ NS/CNT composites used as the anode of LIBs show excellent cyclic performance compared to the pristine $Ca_2Ge_7O_{16}$ NSs and the reported $Ca_2Ge_7O_{16}$ based anodes. The outstanding cycling performance is attributed to the unique synergetic effect in the nanoscale between 1D CNTs and Li^+ hosting 2D NSs. The designed NS structure with high specific surface area provides sufficient electrode-electrolyte contact area and greatly shortens the ionic diffusion length, while CNTs provide high conductance channels. Therefore, it is expected that such a $Ca_2Ge_7O_{16}$ NS/CNT nanocomposite is a highly promising anode material for LIBs. Furthermore, the $Ca_2Ge_7O_{16}$ NS/CNT structure developed here enhance the cycling life can be applicable to other functional nanocomposite materials to improve their cycling stability.

Acknowledgements

We thank National Natural Science Foundation of China (No. 51572058, 91216123, 51174063, 51502057, 51521001), National Basic Research Program of China (2013CB934103, 2012CB933003), the National Natural Science Fund for Distinguished Young Scholars (51425204), the Natural Science Foundation of Heilongjiang Province (E201436, E2016062), the Scientific Research Foundation for the Returned Overseas Chinese Scholars of the State Education Ministry (No. 2015098), the University Nursing Program for Young Scholars with Creative Talents in Heilongjiang province (No. 2015082), the International Science & Technology Cooperation Program of China (2013DFR10630,2015DFE52770) and Specialized Research Fund for the Doctor The acknowledgements come at the end of an article after the conclusions and before the notes and references.

Notes and references

1. M. Armand and J. M. Tarascon, *Nature*, 2008, **451** , 652.
2. B. Dunn, H. Kamath and J. M. Tarascon, *Science*, 2011, **334**, 928.

3. Z. Wang, D. Luan, S. Madhavi and X. W. Lou. *Energy Environ. Sci.,* 2012, **5**, 5252.
4. X. Huang, S. Cui, J. Chang, P. T. Hurley and J. Chen, *Angew. Chem. Int. Ed.* 2015, **54**, 1490.
5. X. Su, Q. Wu, J. Li, X. Xiao and J. Wu. Adv. *Energy Mater*., 2014 , **4**, 1.
6. M. N. Obrovac and V. L. Chevrier. *Chem. Rev.*, 2014, **114**, 11444.
7. T. Kennedy, E. Mullane, H. Geaney, M. Osiak, C. O'Dwyer and K. M. Ryan, *Nano Lett.*, 2014, **14**, 716.
8. L. Y. Lim, S. Fan, H. H. Hng and M. F. Toney, *Adv. Energy Mater.*, 2015, **5**, 1500599.
9. G. Jo, I. Choi, H. Ahn and M. J. Park, *Chem. Commun.*, 2012, **48**, 3987.
10. X. Liu, J. Hao, X. Liu, C. Chi, N. Li, F. Endres, Y. Zhang, Y. Li and J. Zhao, *Chem. Commu.*, 2015, **51** (11), 2064.
11. X. Liu, J. Zhao, J. Hao, B. L. Su and Y. Li, *J. Mater. Chem. A*, 2013, **1**, 15076.
12. J. Hao, X. Liu, X. Liu, X. Liu, N. Li, X. M. Y. Zhang, Y. Li and J. Zhao, *RSC Advances*, 2015, **5** (25), 19596.
13. R. Yi, J. Feng, D. Lv, M. L. Gordin, S. Chen, D. Choi and D. Wang, *Nano Energy*, 2013, **2** (4), 498.
14. W. Li, Di Chen and G. Shen, *J. Mater. Chem. A*, 2015, **3**, 20673.
15. C. H. Kim, Y. S. Jung, K. T. Lee, J. H. Ku and S. M. Oh, *Electrochim. Acta,* 2009, **54**, 4371.
16. J. S. Kim, A. Y. Kim, Y. W. Byeon, J. P. Ahn, D. Byun and J. K. Lee, *Electrochim. Acta*, 2016, **195**, 43.
17. S. Wu, R. Wang, Z. Wang and Z. Lin, *nanoscale*, 2014, **6**, 8350.
18. W. Li, Y. X. Yin, S. Xin, W. G. Song and Y. G. Guo, *Energy Environ. Sci.*, 2012, **5**, 8007.
19. J. K. Feng, C. S. Wang and Y. T. Qian, *Mater. Lett.*, 2014, **122**, 327.
20. S. Jin and C. Wang, *Nano Energy*, 2014, **7**, 63.
21. W. Li, X. Wang, B. Liu, S. Luo, Z. Liu, X. Hou, Q. Xiang, D. Chen and G. Shen, *Chem.-A Eur. J.*, 2013, **19**(26), 8650.
22. D. Li, C. Feng, H. Liu and Z. Guo, *Sci. Rep.*, 2015, **5** , 11326.
23. C. Yuan, L. Yang, L. Hou, L. Shen, X. Zhang and X. W. Lou, *Energy Environ. Sci.*, 2012, **5**, 7883.
24. A. Q. Pan, H. B. Wu, L. Zhang and X. W. Lou, *Energy Environ. Sci.*, 2013, **6**, 1476.
25. C. Ma, W. Zhang, Y. S. He, Q. Gong, H. Che and Z. Feng. Ma, *Nanoscale*, 2016, **8**, 4121.
26. Q. Li, J. Sheng, Q. Wei, Q. An, X. Wei, P. Zhang and L. Mai, *Nanoscale*, 2014, **6**, 11072.
27. F. Zou, X. Hu, Y. Sun, W. Luo, F. Xia, L. Qie, Y. Jiang and Y. Huang, *Chem. Eur. J.*, 2013, **19**, 6027.
28. J. S. Kim, A. Y. Kim, Y. W. Byeon, J. P. Ahn, D. Byun and J. K. Lee, *Electrochim. Acta*, 2016, **195**, 43.
29. Z. Chen, M. Zhou, Y. Cao, X. Ai, H. Yang and J. Liu, J. *Adv. Energy Mater.*, 2012, **2** (1), 95.
30. K. H. Seng, M. Park, Z. P. Guo, H. K. Liu and J. Cho, *Nano Lett.*, 2013, **13**, 1230.
31. S. L. Chou, J. Z. Wang, D. Wexler, K. Konstantinov, C. Zhong, H. K. Liu and S. X. Dou, *J. Mater. Chem.*, 2010, **20**, 2092.
32. L. W. Su, Z. Zhou, X. Qin, Q. W. Tang, D. H. Wu and P. W. Shen, *Nano Energy*, 2013, **2**, 276.
33. D. T. Ngo, H. T. T. Le, R. S. Kalubarme, J. Y. Lee, C. N. Park and C. Park, *J. Mater. Chem. A*, 2015, **3**, 21722.
34. W. He, H. Tian and X. Wang. *J. Mater. Chem. A*, 2015, **3**, 19393.
35. X. Li, J. Liang, Z. Hou, W. Zhang, Y. Wang, Y. Zhu, Y. Qian, *J. Power Sources*, 2015, **293**, 868.

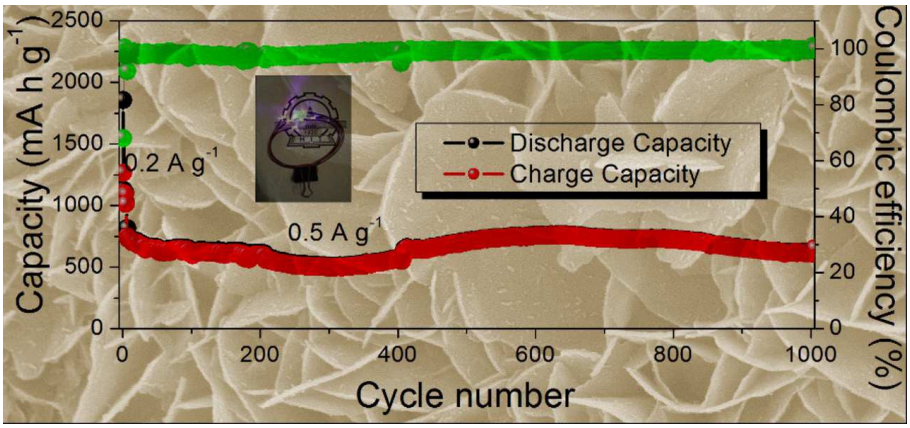

The $Ca_2Ge_7O_{16}$ NS/CNT composites on Ni foam has been successfully fabricated for long cycle lithium-ion batteries.